

Object Classification in 3-D Images Using Alpha-Trimmed Mean Radial Basis Function Network

Adrian G. Borş*and Ioannis Pitas

Department of Informatics

University of Thessaloniki

Thessaloniki 540 06, Greece

Abstract

We propose a pattern classification based approach for simultaneous 3-D object modeling and segmentation in image volumes. The 3-D objects are described as a set of overlapping ellipsoids. The segmentation relies on the geometrical model and graylevel statistics. The characteristic parameters of the ellipsoids and of the graylevel statistics are embedded in a Radial Basis Function (RBF) network and they are found by means of unsupervised training. A new robust training algorithm for RBF networks based on α -trimmed Mean statistics is employed in this study. The extension of the Hough Transform algorithm in the 3-D space by employing spherical coordinate system is used for ellipsoidal center estimation. We study the performance of the proposed algorithm and we present results when segmenting a stack of microscopy images.

*The research reported in this paper had been done while Adrian G. Borş was with Dept. of Informatics, University of Thessaloniki, Greece. Dr. Borş is now with Dept. of Computer Science, University of York, York YO10 5DD, U.K.

1 Introduction

3-D object modeling and segmentation are important tasks in scene processing, understanding and visualization [1, 2, 3]. Several approaches have been adopted in this field and in the following we mention only a few of them. A volumetric image can be seen as an array of voxels at the sites of a 3-D lattice. The main approaches in 3-D object identification consist of representing each object either by a global model description or as a set of component elements. The global description of a 3-D object was considered by using the generalized cylinder model [4] or by minimising an energy function [5, 6]. Modeling 3-D objects by tracking each slice in a stack of images was employed in [7, 8]. The object is represented as a set of generalized cylinders in [6, 8] or as a deformable surface model [9]. The 3-D segmentation in [10] employs a 3-D connectivity algorithm, after appropriate thresholding. Mathematical morphology [11] was used in 3-D domain for segmenting pulmonary trees [12] and brain tissue [13]. Various model-based supervised classifiers have been tested in segmenting 3-D brain images in [14, 15]. Each region is associated with a multivariate Gaussian mixture density in [15]. 3-D modeling from range images using self-organizing maps [16] was employed in [17]. Radial Basis Functions (RBF's) were used for 3-D iterative image reconstruction from projection data in [18] and in 3-D shape from shading reconstruction [19].

In this study we employ an unsupervised classification procedure by using an RBF network for modeling the 3-D scene. The RBF network has a two-layer feed-forward topology and has been successfully employed for functional modeling and pattern classification [20]-[22]. In RBF networks, a function is approximated by a mixture of kernels implemented by the hidden units. The RBF approximation capabilities have been extensively studied [22]-[25]. Due to their functional approximation and localisation properties, RBF's were found attractive for use in computer vision and image processing [26, 27]. Gaussian functions, which geometrically model ellipsoids in 3-D, are used as RBF hidden unit activation functions in the approach described in this study. Mixtures of Gaussian functions have been considered for modeling in many scientific fields. In this approach graylevel and shape are jointly modeled with a set of overlapping Gaussian functions. The input

space consists of four features, denoting the voxel coordinates and the graylevel. The parameters of the ellipsoids can be estimated using the normalized first and second order moments [28]. The calculation of the ellipsoid parameters by using an approach based on moments corresponds to a classical statistical formulation. Their estimation can be performed by means of the k -means clustering algorithm or its adaptive implementation represented by the Learning Vector Quantizer (LVQ) algorithm [16].

A classical training algorithm for RBF networks employs the LVQ algorithm for estimating the Gaussian function parameters [29]. Variants of this algorithm have been derived in order to increase its efficiency in modeling data distributions [26, 30]. An algorithm based on median estimation called Median Radial Basis Function (MRBF) was proved to provide better data classification when compared to the classical algorithm [21]. The classical moment algorithms are sensitive when data are contaminated by noise. In this study we propose a new RBF training algorithm based on the α -trimmed Mean statistics. This algorithm orders the data samples associated with a basis function and eliminates a certain percentage of those situated at the extremes of the distribution. The remaining data is averaged. The α -trimmed Mean algorithm has been proved a good location estimate in the case when data is contaminated with medium and long tailed distributions [31] and has been employed for image filtering [11, 32]. In the approach considered in this study, the number of samples trimmed away from the given distribution depends on the data statistics [33]. The classical RBF and MRBF training algorithms are particular cases of the proposed algorithm. We prove that Alpha-Trimmed Mean RBF algorithm provides unbiased estimates for the ellipses center and this result can be extended for ellipsoids. A trimming algorithm which discards data samples with large Mahalanobis distances from the center is used for covariance matrix estimation [34]. The use of this algorithm for ellipsoid covariance matrix estimation is studied. Experimental results suggest that the proposed algorithm is efficient in estimating parameters of overlapping ellipsoids or when the ellipsoids are embedded in noise.

A study of the similarities among various clustering and energy-minimisation algorithms used

for image boundary extraction is provided in [35]. The Hough Transform has been applied for finding curve parameters in images [28, 36]. In [28], the Hough Transform (HT) is treated in the context of the Bayesian theory. LVQ or other clustering algorithms have been used to estimate the parameters of lines and curves in the Hough space [26, 38]. In this study we propose a 3-D extension of the HT for estimating RBF centers in correspondence with the Alpha-Trimmed Mean RBF algorithm. Various ellipsoids are gathered together, based on the graylevel and location proximity criteria, in order to model complex objects. The Alpha-Trimmed Mean RBF network output parameters are calculated based on the backpropagation algorithm [20, 22]. After estimating the network parameters corresponding to the 3-D modeling, the network can be used to reconstruct the objects or for segmenting 3-D scenes.

The pattern classification criterion employed in this study is described in Section 2. The Alpha-Trimmed Mean RBF algorithm is presented in Section 3 and its application for object modeling in Section 4. Simulation results when applying the proposed algorithm in synthetic object modeling and in 3-D segmentation of a stack of microscopy images are provided in Section 5 and the conclusions are drawn in Section 6.

2 The classification criterion

We employ a Bayesian approach for object classification in volumetric images. Let us denote by \mathcal{O}_k the object to be identified and by \mathcal{F} a 3-D image. The object \mathcal{O}_k which provides the maximum *a posteriori* probability among all the possible candidates is given by :

$$p(\mathcal{O}_k|\mathcal{F}) = \max_{j=1}^M p(\mathcal{O}_j|\mathcal{F}) \quad (1)$$

where M is the total number of objects to be found in the volumetric image. The *a posteriori* probability is expressed by means of Bayesian relationship :

$$p(\mathcal{O}_j|\mathcal{F}) = \frac{p(\mathcal{F}|\mathcal{O}_j) p(\mathcal{O}_j)}{p(\mathcal{F})} \quad (2)$$

where $p(\mathcal{F}|\mathcal{O}_j)$ is the probability associated with 3-D scene modeling from the component objects and $p(\mathcal{O}_j)$ is the *a priori* probability of the object. We decompose these probabilities in a set of components. This corresponds to the fact that a shape can be represented as a combination of several subsets. The relationship (1) becomes :

$$\sum_{m=1}^G [p(g_{mk}) p(\mathcal{F}|g_{mk})] = \max_{j=1}^M \left\{ \sum_{n=1}^G [p(g_{nj}) p(\mathcal{F}|g_{nj})] \right\} \quad (3)$$

where one of the G components making up the object \mathcal{O}_j is denoted as g_{nj} . Each of the component probabilities can be expressed as an energy function :

$$p(\mathcal{F}|g_{nj}) = \frac{1}{Z_{nj}} \exp[-\phi_n(\mathbf{X})] \quad (4)$$

where Z_{nj} is a normalizing constant and $\phi_n(\mathbf{X})$ is a function depending on the feature vectors associated with the voxels. The *a priori* probabilities $p(g_{nj})$ scaled by a constant are taken as weighting factors denoted by λ_{nj} . The relationship (3) can be expressed as :

$$\sum_{m=1}^G \lambda_{mk} \exp[-\phi_m(\mathbf{X})] = \max_{j=1}^M \left\{ \sum_{n=1}^G \lambda_{nj} \exp[-\phi_n(\mathbf{X})] \right\}. \quad (5)$$

This structure is implemented in a Radial Basis Function network. RBF's properties make them suitable to approximate continuous functions with the desired precision [22]-[25]. They are implemented in a two-layer network, where each input represents a feature entry. The hidden-layer unit embeds a Gaussian function :

$$\exp[-\phi_m(\mathbf{X})] = \exp[-(\mathbf{X} - \mu_m)^T \Sigma_m^{-1} (\mathbf{X} - \mu_m)] \quad (6)$$

where μ_m denotes the center vector and Σ_m the covariance matrix. A Gaussian function statistically models a cluster of data and geometrically represents an ellipsoid in 3-D space.

The network output for data vector \mathbf{X} is denoted by $Y_k(\mathbf{X})$ where $k = 1, \dots, M$ and is limited to the interval $(0, 1)$ by a sigmoidal function :

$$Y_k(\mathbf{X}) = \frac{1}{1 + \exp \left(- \sum_{m=1}^G \lambda_{mk} \exp[-\phi_m(\mathbf{X})] \right)}. \quad (7)$$

Each network output is assigned to an object.

3 Alpha-Trimmed Mean Radial Basis Functions

In the previous Section we have expressed the object probabilities as a sum of locally-activated density functions, modeled by Gaussians. Each voxel in the volumetric image is associated to a feature vector consisting of two parts: its coordinates and graylevel respectively, denoted as $\mathbf{X} = [\mathbf{u}, t]$. The Gaussian center is composed of $\mu_m = [\gamma_m, b_m]$, with the former part representing the coordinates of the ellipsoid center in the 3-D image and the latter its characteristic graylevel. The cross-correlation between the features denoting the coordinates and the graylevel is set to zero. The covariance matrix associated to the basis function is :

$$\Sigma = \begin{pmatrix} \mathbf{S} & \mathbf{0} \\ \mathbf{0} & v \end{pmatrix} \quad (8)$$

where \mathbf{S} models the shape and represents a 3×3 matrix in 3-D and v is the graylevel variance. Thus, the function (6) can be decomposed in :

$$\exp[-\phi_m(\mathbf{X})] = \exp[-(\mathbf{u} - \gamma_m)^T \mathbf{S}_m^{-1} (\mathbf{u} - \gamma_m)] \exp \left[- \left(\frac{t - b_m}{v_m} \right)^2 \right] \quad (9)$$

where the first expression of the decomposition is associated to the geometry of the object and the second to the graylevel distribution. This model is embedded in an RBF network.

A classical approach in training RBF networks employs the LVQ algorithm [16] for estimating the hidden unit function center [29]. Similar training algorithms for RBF networks have been considered for curve parameter estimation [26] and channel equalization [30]. These algorithms correspond to the classical statistics theory and provide unbiased results if the distributions are Gaussian and non-overlapping.

The algorithm proposed in this study is based on an unsupervised approach, similar to the LVQ. We generate a set of centers at random and the algorithm calculates the Euclidean distance from a data sample to each of them. The closest center to the given data vector is chosen to be updated :

$$\|\mathbf{X} - \mu_k\| = \min_{i=1}^G \|\mathbf{X} - \mu_i\| \quad (10)$$

where μ_k is the closest center to the incoming data sample \mathbf{X} . A robust statistics based algorithm employing the marginal median for Gaussian center estimation and the median of the absolute

deviation from the median for width estimation and called Median RBF (MRBF) was proposed in [21]. The theoretical analysis has shown that the bias provided by MRBF is smaller than that of the classical LVQ-based RBF algorithm when estimating the parameters of a mixture of overlapping Gaussians. In this study, a new robust statistics based training algorithm which contains the previous two approaches as particular cases is proposed. Data samples assigned to a specific cluster according to (10) are arranged in the order of their values on each dimension independently. Let us denote them in correspondence to their rank as $X_{(i)}$ for $i = 1, \dots, N_k$ where N_k is the total number of data samples assigned to the k -th hidden unit. A very general description of many robust statistics algorithms assigns a weight to each data sample with respect to its rank [31, 37] :

$$\hat{\mu}_k = \frac{\sum_{i=1}^{N_k} W_i X_{(i)}}{\sum_{i=1}^{N_k} W_i} \quad (11)$$

where W_i is the weight depending on the ranking of the respective data sample. If $W_i = 1$ for $i = 1, \dots, N_k$, then the center is computed by averaging. If $W_i = 0$ for $i = 1, \dots, \lfloor \frac{N_k}{2} \rfloor - 1$, $i = \lfloor \frac{N_k}{2} \rfloor + 1, \dots, N_k$, and $W_i = 1$ for $i = \lfloor \frac{N_k}{2} \rfloor$ we obtain the marginal median estimator. In other robust statistics algorithms, W_i is replaced by a function which decreases with respect to the distance of the data sample $X_{(i)}$ from the central ordered data sample $X_{(\lfloor \frac{N_k}{2} \rfloor)}$. In this study we propose to use the α -trimmed Mean algorithm [11, 31] which assigns $W_i = 1$ for $i = \alpha_k N_k, \dots, N_k - \alpha_k N_k$, and $W_i = 0$ for the rest of data samples, where α_k is the percentage of data samples to be trimmed away at each extreme of the k -th hidden unit data distribution. The α -trimmed Mean algorithm is a good choice for long and medium tail data distributions and has been extensively used for image filtering [11, 32]. The adaptive implementation of the algorithm updates the parameters of a basis function using only the data samples which are inside of a certain range of ranked samples :

$$\hat{\mu}_{k,t} = \begin{cases} \hat{\mu}_{k,t-1} + \frac{\mathbf{X}_{(i)} - \hat{\mu}_{k,t-1}}{N_{k,t} - 2\alpha_k N_{k,t}} & \text{if } \alpha_k N_{k,t} < i \leq N_{k,t} - \alpha_k N_{k,t} \\ \hat{\mu}_{k,t-1} & \text{otherwise} \end{cases} \quad (12)$$

where $\hat{\mu}_{k,t}$ and $N_{k,t}$ denote the center estimate and the number of data samples assigned to the k -th basis function at the moment t . We can observe that for $\alpha_k=0$ we obtain the LVQ algorithm for

minimum output variance [39].

The parameter α_k is chosen according to the data distribution. The following measure is used for estimating the tail length of the data distribution [33] :

$$Q = \frac{U[0.5] - L[0.5]}{U[0.05] - L[0.05]} \quad (13)$$

where $U[\beta]$, $L[\beta]$ represent the average of the upper and respectively the lower β percent of data samples assigned to a specific basis function. The number of data samples to be trimmed away relies directly on the value of Q :

$$\hat{\alpha}_k = \frac{1 - Q}{2}. \quad (14)$$

For long tailed distributions, the amount of data samples to be trimmed is large while for short tailed distributions less samples are trimmed away.

For the second order statistics, we order the data samples assigned to a basis function according to their Mahalanobis distance from the estimated center $\hat{\mu}_k$, starting with :

$$\mathcal{M}_{(1)} = \min_{i=1}^{N_k} [(\mathbf{X}_i - \hat{\mu}_k)^T \hat{\Sigma}_k^{-1} (\mathbf{X}_i - \hat{\mu}_k)]. \quad (15)$$

After ordering the data samples assigned to the k -th basis function according to this measure $\mathbf{X}_{(1),\mathcal{M}} < \dots < \mathbf{X}_{(i),\mathcal{M}}$, the estimate of the covariance matrix is obtained using ellipsoidal trimming [34] :

$$\hat{\Sigma}_k = \frac{\sum_{i=1}^{N_k - \alpha_{k,\mathcal{M}} N_k} (\mathbf{X}_{(i),\mathcal{M}} - \hat{\mu}_k) (\mathbf{X}_{(i),\mathcal{M}} - \hat{\mu}_k)^T}{N_k - \alpha_{k,\mathcal{M}} N_k} \quad (16)$$

where $\mathbf{X}_{(i),\mathcal{M}}$ denotes the i -th ordered data sample according to the Mahalanobis distance (15) and $\alpha_{k,\mathcal{M}}$ is the trimming percentage in this case. Similarly with (12) this formula can also be implemented in an adaptive form. The formula (16) corresponds to peeling off observations in shells using a sequence of convex hulls. The formulae (12) and (16) make up the Alpha-Trimmed Mean RBF training algorithm.

4 Object modeling using Alpha-Trimmed Mean RBF

In this Section we study the application of the Alpha-Trimmed Mean RBF algorithm for estimating the parameters of ellipsoids. The analytic form of an ellipsoid is :

$$(\mathbf{u} - \boldsymbol{\gamma})^T \mathbf{S}^{-1} (\mathbf{u} - \boldsymbol{\gamma}) \leq 1. \quad (17)$$

We can observe that the ellipsoid center and width correspond to the mean and variance of a Gaussian function. The orientation of the ellipsoid can be derived from the components of the Gaussian covariance matrix. Algorithms based on first and second order moments are used for calculating the ellipse parameters [28] and they can be extended for ellipsoids. However, the classical moment-based method is likely to provide a biased estimate in the case when ellipsoids are overlapping or in the presence of noise.

For simplifying the notation let us consider an ellipse as the 2-D case of an ellipsoid. The calculation of the center using (12) is done on each dimension independently and does not depend on the number of entries. The pixels of the ellipse are uniformly distributed in the domain defined by (17). The center of the ellipse is estimated from the normalized first order moments :

$$E[\hat{\gamma}_x] = \frac{\int_{-\infty}^{\infty} \int_{-\infty}^{\infty} x f(x, y) dx dy}{\int_{-\infty}^{\infty} \int_{-\infty}^{\infty} f(x, y) dx dy} = \frac{\int_{x_{inf}}^{x_{sup}} \int_{y_{inf}}^{y_{sup}} x dy dx}{\int_{x_{inf}}^{x_{sup}} \int_{y_{inf}}^{y_{sup}} dy dx} \quad (18)$$

where $f(x, y)$ denotes the distribution function of the truncated ellipse and $x_{inf}, y_{inf}, x_{sup}, y_{sup}$ its limits, $\hat{\gamma}_x$ denotes the estimate of the center vector component on the x axis. The denominator in (18) calculates the area of the ellipse after truncation. In Figure 1 the truncation of an ellipse by α -trimmed Mean algorithm is displayed.

The following proposition has been proved in Appendix A :

Proposition 4.1 *The center of an ellipse is exactly determined after ordering the corresponding data samples of its distribution and after trimming away an α percentage of them at both limits, $\forall \alpha \in [0, \frac{1}{2})$.*

For the ellipse covariance matrix we calculate the normalized second order moments for the distribution left after trimming :

$$E[\hat{\mathbf{S}}] = \frac{\int_{-\infty}^{\infty} \int_{-\infty}^{\infty} (\mathbf{u} - \hat{\gamma})(\mathbf{u} - \hat{\gamma})^T f_{\mathcal{M}}(x, y) dx dy}{\int_{-\infty}^{\infty} \int_{-\infty}^{\infty} f_{\mathcal{M}}(x, y) dx dy} = \frac{\int_{x_{inf, \mathcal{M}}}^{x_{sup, \mathcal{M}}} \int_{y_{inf, \mathcal{M}}}^{y_{sup, \mathcal{M}}} (\mathbf{u} - \hat{\gamma})(\mathbf{u} - \hat{\gamma})^T dx dy}{\int_{x_{inf, \mathcal{M}}}^{x_{sup, \mathcal{M}}} \int_{y_{inf, \mathcal{M}}}^{y_{sup, \mathcal{M}}} dy dx} \quad (19)$$

where $f_{\mathcal{M}}(x, y)$ is the function describing the ellipse, trimmed based on (16), and $x_{inf, \mathcal{M}}$, $y_{inf, \mathcal{M}}$, $x_{sup, \mathcal{M}}$, $y_{sup, \mathcal{M}}$ denote the geometrical limits of the ellipse after trimming. The illustration of ellipse trimming by excluding from computation extreme shells of data is displayed in Figure 2. Evidently, when trimming data samples from an ideal ellipse, a smaller covariance matrix is obtained. The loss of data must be compensated in certain cases. In Appendix B the estimation of the covariance matrix after trimming an ideal ellipse is studied. The conclusion of this study is the following :

Proposition 4.2 *The variance of an ellipse after trimming is given by :*

$$\hat{\mathbf{S}}_k = \frac{\sum_{i=1}^{N_k - \alpha_{k, \mathcal{M}} N_k} (\mathbf{u}_{(i), \mathcal{M}} - \hat{\gamma}_k) (\mathbf{u}_{(i), \mathcal{M}} - \hat{\gamma}_k)^T}{(1 - \alpha_{k, \mathcal{M}})^2 N_k} \quad (20)$$

where $\mathbf{u}_{(i), \mathcal{M}}$ is the i -th location vector ordered according to the Mahalanobis distance from the center of the ellipse and $\alpha_{k, \mathcal{M}}$ is the percentage of trimmed data samples associated with the k -th basis function.

From the formulae (15,16) we can observe that the estimation of the covariance matrix by trimming does not depend on a specific dimension or on the number of dimensions. The conclusions provided in Proposition 4.1 and Proposition 4.2 for ellipses can be extended for ellipsoids as well.

When estimating an elliptical shape, formula (20) corresponds to the redistribution of the data samples associated with the ellipse such that its distortions are compensated. The α -trimmed Mean algorithm has been shown as robust when estimating data corrupted by noise [11, 31, 32, 33, 34]. In order to analyse the capabilities of shape estimation for the Alpha-Trimmed Mean RBF algorithm, a distorted elliptic shape is shown in Figure 3a. The ellipse estimated by the classical moments method [28] and by the proposed Alpha-Trimmed Mean RBF algorithm are shown in Figure 3b and

in Figure 3c. It can be observed that Alpha-Trimmed Mean RBF algorithm is robust in estimating the ellipse parameters when data is distorted by noise.

In order to model the geometrical shape by the basis functions we can employ a 3-D extension of the Hough Transform (3-D HT) in combination with the Alpha-Trimmed Mean RBF algorithm. HT represents a mapping from the image features to sets of points in a parameter space [2, 28, 36]. The parameters provided by the Hough Transform have been used as input features for the RBF and LVQ algorithms, in order to detect lines [26] and for texture classification [38]. For voxels where a significant edge is located, we generate a set of parameters which are compatible with the volumetric image features and the hypothesized model. The Hough Transform can be used to detect complex parametric curves [28, 36]. However, the number of required parameters increases with respect to the complexity of the model. In order to reduce the computational complexity, HT is employed only for finding estimates of sphere centers to be used in the context of the Alpha-Trimmed Mean RBF algorithm. For finding the object edges we apply a 3-D extension of the Sobel edge detector algorithm which provides both edge intensity and orientation. The transformation from the rectangular to the spherical coordinate system is given by the system of equations :

$$r = \sqrt{x^2 + y^2 + z^2} \quad (21)$$

$$\theta = \arctan\left(\frac{x}{y}\right) \quad (22)$$

$$\psi = \arctan\left(\frac{z}{\sqrt{x^2 + y^2}}\right) \quad (23)$$

where (r, θ, ψ) are the spherical coordinates corresponding to a voxel $\mathbf{u} = (x, y, z)$ in the rectangular coordinate system. After the 3-D Sobel edge calculation, the orientation θ_e of the edge with respect to the plane (x, y) is given by a formula based on (22) and the orientation ψ_e with respect to z axis is derived from (23). We consider a certain volumetric image partition in cubes and we associate an accumulator ε to each cube. The possible candidates for the centers of the component spheres can be expressed with respect to the locations of significant edges (x_e, y_e, z_e) as :

$$x = x_e + r \cos(\psi_e) \cos(\theta_e) \quad (24)$$

$$y = y_e + r \cos(\psi_e) \sin(\theta_e) \quad (25)$$

$$z = z_e + r \sin(\psi_e) \quad (26)$$

for a certain interval $r = (0, R)$. For each r from the given interval we increment the accumulator ε corresponding to all the points (x, y, z) as provided by (24)-(26). From (9) we observe that we can train separately the RBF weight components modeling the geometrical shape γ, \mathbf{S} and the graylevel variance v . We use the accumulators provided by 3-D HT as weights in the adaptive Alpha-Trimmed Mean RBF for estimating centers of spheres :

$$\hat{\gamma}_{k,t} = \begin{cases} \hat{\gamma}_{k,t-1} + \frac{\varepsilon_i \mathbf{u}_{(i)} - \varepsilon_k \hat{\gamma}_{k,t-1}}{N_k - \alpha_k N_k} & \text{if } \alpha_k N_k < i < N_k - \alpha_k N_k \\ \sum_{i=\alpha_k N_k} \varepsilon_i & \\ \hat{\gamma}_{k,t-1} & \text{otherwise} \end{cases} \quad (27)$$

where ε_i is the accumulator associated with the voxel location $\mathbf{u}_{(i)}$. For the graylevel feature, considering the decomposition property (9), we can use the relationship (12). The larger accumulators ε_i correspond to bigger probabilities that a sphere center is located there. The result of the Alpha-Trimmed Mean RBF given by (27) will be weighted towards the sphere center as provided by the 3-D HT estimates. In this case, the ordering considers the product of the coordinate location and its respective accumulator $\varepsilon_i \mathbf{u}_{(i)}$. In the case of ideal ellipsoids this produces a function with an elliptic support that is symmetrically distributed with respect to its center. We can observe that the result provided by Proposition 4.1 is valid in this situation as well.

Complex objects in images can be modeled by using shape decomposition based on mathematical morphology [36] or overlapping Gaussian functions [19]. As a consequence of RBF function modeling capabilities [22]-[25], geometrically any continuous object can be represented by a certain number of ellipsoids with a given accuracy. By combining graylevel and geometrical information we can model objects which do not have smooth boundaries. Very irregular objects would require a large number of ellipsoids in order to be modeled. After estimating the hidden-unit parameters according to (27) and (20) we calculate the output parameters λ_{mk} . These weights denote the association among the hidden and output units. Positive λ_{mk} 's correspond to ellipsoids which are added in order to model

objects and negative λ_{mk} 's correspond to holes (missing parts) in objects. Usually the output weights are estimated based on *a priori* assumptions [22]. In this study we have applied an unsupervised approach similar to that used for describing moving objects in image sequences [27]. The voxels are assigned to a certain set H_m associated with a hidden unit k , after evaluating (12,27,20) :

$$H_m = \{\mathbf{X} \mid \exp[-\phi_m(\mathbf{X})] = \max_{i=1}^G \exp[-\phi_i(\mathbf{X})]\} \quad (28)$$

where $\exp[-\phi(\mathbf{X})]$ is provided in (6). In order to group various ellipsoids in distinct objects we employ two criteria: the first criterion considers the geometrical compactness and the second takes into account the similarity in the graylevel statistics. In the second criterion only the data samples assigned to the neighbouring region pairs are considered. The compactness is calculated based on the cardinality between the regions associated to each two hidden units [40] :

$$V(H_m, H_n) = \sum_{(x,y,z) \in H_m} |\mathcal{N}_{xyz} \cap H_n| \quad (29)$$

where H_m and H_n are the sets associated with two hidden units, $|\cdot|$ denotes the cardinal operation and \mathcal{N}_{xyz} is a 27 voxel neighbourhood of the site (x, y, z) containing the labels of the respective voxels. This measure calculates the border length between the volumes assigned to two different basis functions [27]. If $V(H_m, H_n) \neq 0$, then we evaluate the similarity in the graylevel distribution and compare it with a certain threshold. Let us denote by $f_m(b)$ the distribution of the graylevel statistics corresponding to H_m , calculated as a histogram. The similarity is evaluated as the distance between the normalized graylevel distributions associated to the two regions :

$$\text{If } \sum_{b=0}^{255} \left| \frac{f_m(b)}{N_m} - \frac{f_n(b)}{N_n} \right| < h \text{ then } \begin{cases} F_k(\mathbf{X}) = 1 & \forall \mathbf{X} \in H_n, \forall \mathbf{X} \in H_m \\ F_j(\mathbf{X}) = 0 & \forall j \neq k \end{cases} \quad (30)$$

where h is a threshold and $F_k(\mathbf{X})$ is a decision function for the class k which contains the sets H_m, H_n . If h is small, the 3-D scene will be split in many objects and if it is big, then fewer objects will be considered. $F_k(\mathbf{X})$ are used as target labels for estimating the output parameters. We use the backpropagation algorithm for finding the output parameters [22] :

$$\lambda_{mk} = \sum_{\mathbf{X}} [F_k(\mathbf{X}) - Y_k(\mathbf{X})] Y_k(\mathbf{X}) [1 - Y_k(\mathbf{X})] \phi_m(\mathbf{X}) \quad (31)$$

where $Y_k(\mathbf{X})$ is the output provided by the network (7) and $F_k(\mathbf{X})$ is the data target label decided according to (30). The object borders coincide with the classification boundary between their class discriminant functions, as it is provided by the Bayesian classification theory described in Section 2. The parameters of the 3-D scene are thus embedded in the network. The hidden units model the characteristics of the ellipsoids and the output units represent objects. The presentation of the 3-D object modeling and segmentation algorithm is shown in Figure 4. The training algorithm for Alpha-Trimmed Mean RBF algorithm in the context of 3-D object modeling is detailed in Figure 5.

5 Simulation results

The Alpha-Trimmed Mean RBF algorithm has been tested in many applications. We have used the Alpha-Trimmed Mean RBF algorithm as described in Section 3, when modeling a synthetic object. We consider the modeling of a 3-D shape consisting of six spheres of constant intensity with the centers located at $(40,50,50)$, $(60,50,50)$, $(50,40,50)$, $(50,60,50)$, $(50,50,40)$, $(50,50,60)$. The resulting shape is displayed in Figure 6a. The coordinates of the voxels composing the shape are considered as inputs in the neural network. After applying the formulae (12) and (20) we obtain the parameters describing the given object. Afterwards, the shape is reconstructed from the parameters embedded in the neural network. The modeling results when using RBF, Alpha-Trimmed Mean RBF and MRBF network are displayed in Figures 6 b, c, and d. We distort the shape of the artificial object by adding noise. The noise is uniformly distributed in the volume $[0, 100] \times [0, 100] \times [0, 100]$ and has probability of occurrence 0.2 % in the entire volume. In the locations where the noisy samples are added, the pixel values are switched from the level of the object to that of the background and vice versa. The noisy image is displayed in Figure 7a. The objects reconstructed based on the classical training algorithm for RBF, Alpha-Trimmed Mean RBF and MRBF algorithm are displayed in Figures 7 b, c, d. Two measures are considered for numerical comparison. The first error criterion measures the

average bias in center location :

$$E = \frac{1}{G} \sum_{k=1}^G \|\mu_k - \hat{\mu}_k\|^2 \quad (32)$$

where $G = 6$ represents the number of spheres and $\mu_k, \hat{\mu}_k$ are the original and the estimated location of centers respectively. A second measure is the volume error and it is calculated as the absolute difference between the volume of the original shape (Figure 6a) and the volume representing the object reconstructed based on the estimated parameters, normalized at the size of the original object. The average of the results when applying several times RBF, MRBF and Alpha-Trimmed Mean RBF are provided in Table 1. We can observe from this Table as well as from Figures 6 and 7 that Alpha-Trimmed Mean RBF provides a better result than that of RBF when estimating the original shape from Figure 6a, and better modeling capabilities than MRBF when estimating the parameters from the noisy shape. These results show the capability of the proposed algorithm to model a composite shape as well as its robustness to noise corruption.

The algorithm described in Section 4 has been applied for segmenting 3-D images. We present here a test on a stack of 60 microscopy images, representing blood vessels in tooth pulp. The images composing the stack represent parallel and equidistant cross-sections through the object structure. A set of nine frames is presented in Figure 8. A rendered volumetric view of the stack of images is shown in Figure 11a. We intend to segment the blood vessels represented as continuous darker areas. As can be observed in these images, the tissue structure is very noisy and the objects are not well defined. Some of the images contain darker or lighter patterns caused by inappropriate image acquisition. Most of the algorithms employed for segmentation of similar images rely on semiautomatic operations involving manual operations [1]. In the training stage we have used only 20 frames (one out of each three consecutive frames) and the features were extracted from 16×16 pixel blocks. This ensured a great reduction in the number of input data samples and, implicitly, in the training time. We have not employed any preprocessing stage involving alignment or luminance equalization. For modeling the objects we apply the procedures as described in the flows from Figures 4 and 5. After the 3-D extension of the Sobel edge detector, we compute the 3-D

Hough Transform. Initially we consider a certain number of hidden units and those which have been assigned with few data samples according to (10) are afterwards discarded. The voxel coordinates weighted by the accumulator cells provided by the 3-D HT and the graylevel are used for modeling the 3-D object shape and structure. The data samples associated with various hidden-units and corresponding to component parts of the objects are organized in data histograms. A segmentation which relies only on the graylevel value would provide spurious patterns all across the image. If the segmentation would rely only on the geometrical shape, the borders of the objects would not be accurately represented or the number of required ellipsoids would be very high. The neighbouring 3-D regions which are defined by estimating the hidden-unit parameters, are joined together based on their graylevel similarities. Correspondences among the 3-D regions modeled by the hidden units and the 3-D objects are given by the output weights λ_{mk} . After estimating the location, shape and the graylevel parameters, we apply the network on the entire stack of 60 images, on 2×2 pixel blocks. The segmentation of the frames from Figure 8 using RBF and Alpha-Trimmed Mean RBF is shown in Figures 9 and 10, respectively. As it can be observed from Figure 10, the segmentation of the two blood vessels is good and the spurious patterns scattered around the objects are greatly reduced when using the Alpha-Trimmed Mean RBF algorithm. The 3-D segmentation of the two blood vessels is completely automatic. The Alpha-Trimmed Mean RBF segmentation result is visualized for various perspective angles in Figures 11 b, c and d.

6 Conclusions

In this study we propose a new algorithm for modeling and segmenting 3-D objects. We employ a classification-based procedure which uses as inputs the graylevel and the voxel coordinates. In this study the objects are composed of overlapping ellipsoids. The classifier employed in modeling the 3-D structure as well as the graylevel is the RBF network, where each basis unit corresponds to an ellipsoid. We provide a robust learning algorithm for RBF network based on the α -Trimmed Mean statistics. This algorithm trims away a number of data samples according to the data statistics. We

prove that the Alpha-Trimmed Mean RBF algorithm provides no bias when estimating the center of an ellipse and we derive the formula for estimating the ellipses covariance matrix after trimming. The extension of the conclusions for ellipsoids is straightforward. In order to find the centers of the ellipsoids we develop a 3-D Hough Transform which is integrated in the Alpha-Trimmed Mean RBF training algorithm. The network parameters embed location, shape and graylevel information of the objects. Each output of the network corresponds to an object.

Appendix A

Let us denote the components of the covariance matrix from (17) as :

$$\mathbf{S}^{-1} = \begin{pmatrix} a & c \\ c & b \end{pmatrix}. \quad (33)$$

In order to evaluate the limits of integration in (18) we calculate the tangents at the ellipse parallel with y direction :

$$x_t = \gamma_x + \frac{(\mathbf{S}\mathbf{v})_x}{\sqrt{\mathbf{v}^T \mathbf{S} \mathbf{v}}} \quad (34)$$

where $(\mathbf{S}\mathbf{v})_x$ denotes the x component of $\mathbf{S}\mathbf{v}$ and \mathbf{v} is the vector normal to ellipse and parallel with the x axis [28]. After choosing two vectors $\mathbf{v}_1 = (1 \ 0)^T$ and $\mathbf{v}_2 = (-1 \ 0)^T$ we derive the limits on the x axis. Let us denote with x_α the interval from ellipse, measured along the x axis, which is going to be eliminated by trimming an α percentage at each extremity of the data distribution. The integration limits corresponding to the truncated ellipse are :

$$x_{sup}, x_{inf} = \gamma_x \pm \left(x_\alpha - \sqrt{\frac{b}{ab - c^2}} \right) \quad (35)$$

The integration limits on the y axis are derived with respect to x coordinates when considering equality in (17) :

$$y_{sup}, y_{inf} = \gamma_y + \frac{-c(x - \gamma_x) \pm \sqrt{b - (ab - c^2)(x - \gamma_x)^2}}{b} \quad (36)$$

The denominator of the expression (18), representing the area of the truncated ellipse, can be expressed, after changing the variable, and considering (35,36) as :

$$\int_{x_{inf}}^{x_{sup}} \int_{y_{inf}}^{y_{sup}} dy dx = \frac{2}{\sqrt{ab - c^2}} \int_{-1+x_\alpha\sqrt{(ab-c^2)/b}}^{1-x_\alpha\sqrt{(ab-c^2)/b}} \sqrt{1 - z^2} dz \quad (37)$$

Similarly, the numerator from (18) is :

$$\begin{aligned} \int_{x_{inf}}^{x_{sup}} \int_{y_{inf}}^{y_{sup}} x dy dx &= \frac{2\gamma_x}{\sqrt{ab - c^2}} \int_{-1+x_\alpha\sqrt{(ab-c^2)/b}}^{1-x_\alpha\sqrt{(ab-c^2)/b}} \sqrt{1 - z^2} dz + \\ &\frac{2\sqrt{b}}{ab - c^2} \int_{-1+x_\alpha\sqrt{(ab-c^2)/b}}^{1-x_\alpha\sqrt{(ab-c^2)/b}} z \sqrt{1 - z^2} dz. \end{aligned} \quad (38)$$

The second integral in (38) is zero and the result of the estimation is :

$$E[\hat{\gamma}_x] = \frac{\int_{x_{inf}}^{x_{sup}} \int_{y_{inf}}^{y_{sup}} x dy dx}{\int_{x_{inf}}^{x_{sup}} \int_{y_{inf}}^{y_{sup}} dy dx} = \gamma_x, \forall \alpha \in \left[0, \frac{1}{2}\right). \quad (39)$$

Appendix B

The equation of the ellipse resulted after ordering the data samples assigned to a basis function according to the Mahalanobis distance from the center (15) and trimming a percentage $\alpha_{\mathcal{M}}$ is :

$$(\mathbf{u} - \boldsymbol{\gamma})^T \mathbf{S}^{-1} (\mathbf{u} - \boldsymbol{\gamma}) = 1 - \alpha_{\mathcal{M}} \quad (40)$$

Following a similar derivation as in Appendix A, we obtain the integration limits on x axis :

$$x_{sup,\mathcal{M}}, x_{inf,\mathcal{M}} = \gamma_x \pm \sqrt{\frac{b(1 - \alpha_{\mathcal{M}})}{ab - c^2}} \quad (41)$$

Similarly with (36) we derive the integration limits for y axis. The area of the ellipse after trimming is :

$$\int_{x_{inf,\mathcal{M}}}^{x_{sup,\mathcal{M}}} \int_{y_{inf,\mathcal{M}}}^{y_{sup,\mathcal{M}}} dy dx = \frac{(1 - \alpha_{\mathcal{M}})\pi}{\sqrt{ab - c^2}} \quad (42)$$

For one of the covariance matrix components from the numerator in the expression (20) we obtain :

$$\int_{x_{inf,\mathcal{M}}}^{x_{sup,\mathcal{M}}} \int_{y_{inf,\mathcal{M}}}^{y_{sup,\mathcal{M}}} (x - \gamma_x)^2 dy dx = \frac{(1 - \alpha_{\mathcal{M}})^2 b}{\sqrt{(ab - c^2)^3}} \int_{-1}^1 z^2 \sqrt{1 - z^2} dz = \frac{(1 - \alpha_{\mathcal{M}})^2 \pi b}{4\sqrt{(ab - c^2)^3}} \quad (43)$$

From (42) and (43) we derive the estimate for the variance on x axis :

$$\frac{\int_{x_{inf,\mathcal{M}}}^{x_{sup,\mathcal{M}}} \int_{y_{inf,\mathcal{M}}}^{y_{sup,\mathcal{M}}} (x - \gamma_x)^2 dy dx}{\int_{x_{inf,\mathcal{M}}}^{x_{sup,\mathcal{M}}} \int_{y_{inf,\mathcal{M}}}^{y_{sup,\mathcal{M}}} dy dx} = \frac{(1 - \alpha_{\mathcal{M}})b}{4(ab - c^2)} \quad (44)$$

We obtain similar expressions for the other components of the covariance matrix in the numerator from (20). We observe that for $\alpha_{\mathcal{M}} = 0$ in (44) we obtain the same ellipse width estimate as that provided in the case of the ideal ellipse when using the classical normalized second order moment method [28].

References

- [1] C. Roux, J.-L. Coatrieux, *Contemporary Perspectives in Three-Dimensional Biomedical Imaging*. Amsterdam: IOS Press, 1997.
- [2] O. Faugeras, *Three-dimensional Computer Vision, A Geometrical Viewpoint*, Cambridge, MA: MIT Press, 1993.
- [3] G. Lohman, *Volumetric image analysis*. J. Wiley-Teubner, 1998.
- [4] J. Ponce, D. Chelberg, W. M. Mann, "Invariant properties of straight homogeneous generalized cylinders and their contours," *IEEE Trans. on Pattern Analysis and Machine Intelligence*, vol. 11, no. 9, pp. 951-966, 1989.
- [5] L. D. Cohen, I. Cohen, "Finite-element methods for active contour models and balloons for 2-D and 3-D images," *IEEE Trans. on Pattern Analysis and Machine Intelligence*, vol. 15, no. 11, pp. 1131-1147, 1993.
- [6] B. Verdonck, I. Bloch, H. Maître, D. Vandermeulen, P. Suetens, G. Marchal, "Accurate segmentation of blood vessels from 3D medical images," *Proc. IEEE International Conference on Image Processing*, Lausanne, Switzerland, vol. III, pp. 311-314, 1996.
- [7] V. Burdin, C. Roux, C. Lefèvre, E. Stindel, "Modeling and analysis of 3-D elongated shapes with applications to long bone morphometry," *IEEE Trans. on Medical Imaging*, vol. 15, no. 1, pp. 79-91, 1996.
- [8] Q. Huang, G. C. Stockman, "Generalized stochastic tube model: tracking 3D blood vessels in MR images," *Proc. International Conference on Pattern Recognition*, Jerusalem, Israel, pp. 156-160, 1994.
- [9] C. Davatzikos, R. N. Bryan, "Using a deformable surface model to obtain a shape representation of the cortex," *IEEE Trans. on Medical Imaging*, vol. 15, no. 6, pp. 785-801, 1996.

- [10] M. Joliot, B. M. Mazoyer, "Three-dimensional segmentation and interpolation of magnetic resonance brain images," *IEEE Trans. on Medical Imaging*, vol. 12, no. 2, pp. 269-277, 1993.
- [11] I. Pitas, A. N. Venetsanopoulos, *Nonlinear Digital Filters: principles and applications*. Norwell, MA: Kluwer Academic, 1990.
- [12] C. Pisupati, L. Wolff, E. Zerhouni, W. Mitzner, "Segmentation of 3D pulmonary trees using mathematical morphology," *Proc. Mathematical Morphology and its Applications to Image and Signal Processing*, Atlanta, pp. 409-416, 1996.
- [13] J. Madrid, N. Ezquerro, "Automatic 3-dimensional segmentation of MR brain tissue using filters by reconstruction," *Proc. Mathematical Morphology and its Applications to Image and Signal Processing*, Atlanta, pp. 417-424, 1996.
- [14] M. Kamber, R. Shinghal, D. L. Collins, G. S. Francis, A. C. Evans, "Model-based 3-D segmentation of multiple sclerosis lesions in magnetic resonance brain images," *IEEE Trans. on Medical Imaging*, vol. 14, no. 3, pp. 442-453, Sep. 1995.
- [15] A. Lundervold, G. Stovik, "Segmentation of brain parenchyma and cerebrospinal fluid in multispectral magnetic resonance images," *IEEE Trans. on Medical Imaging*, vol. 14, no. 2, pp. 339-349, June 1995.
- [16] T. Kohonen, *Self Organization and Associative Memory*. Berlin: Springer-Verlag, 1988.
- [17] S.-W. Chen, G. C. Stockman, K.-E. Chang, "SO dynamic deformation for building of 3-D models," *IEEE Trans. on Neural Networks*, vol. 7, no. 2, pp. 374-387, March 1996.
- [18] S. Matej, R. M. Lewitt, "Practical considerations for 3-D image reconstruction using spherically symmetric volume elements," *IEEE Trans. on Medical Imaging*, vol. 15, no. 1, pp. 68-78, 1996.
- [19] G.-Q. Wei, G. Hirzinger, "Parameteric shape-from-shading by radial basis functions," *IEEE Trans. on Pattern Analysis and Machine Intelligence*, vol. 19, no. 4, pp. 353-365, 1997.

- [20] A. G. Bors, M. Gabbouj, "Minimal topology for a radial basis functions neural network for pattern classification," *Digital Signal Processing: A review journal*, vol. 4, no. 3, pp. 173-188, July 1994.
- [21] A. G. Bors, I. Pitas, "Median radial basis function neural network," *IEEE Trans. on Neural Networks*, vol. 7, no. 6, pp. 1351-1364, 1996.
- [22] S. Haykin, *Neural Networks: A Comprehensive Foundation*. Upper Saddle River, NJ: Prentice Hall, 1994.
- [23] E. J. Hartman, J. D. Keeler, J. M. Kowalski, "Layered neural networks with Gaussian hidden units as universal approximations," *Neural Computation*, vol. 2, pp. 210-215, 1990.
- [24] J. Park, J. W. Sandberg, "Universal approximation using radial basis functions network," *Neural Computation*, vol. 3, pp. 246-257, 1991.
- [25] T. Poggio, F. Girosi, "Networks for approximation and learning," *Proc. of the IEEE*, vol. 78, no. 9, pp. 1481-1497, Sep. 1990.
- [26] L. Xu, A. Krzyzak, E. Oja, "Rival penalized competitive learning for clustering analysis, RBF net, and curve detection," *IEEE Trans. on Neural Networks*, vol. 4, no. 4, pp. 636-649, July 1993.
- [27] A. G. Bors, I. Pitas, "Optical flow estimation and moving object segmentation based on MRBF network," *IEEE Trans. on Image Processing*, vol. 7, no. 5, pp. 693-702, May 1998.
- [28] R.M. Haralick, L.G. Shapiro, *Computer and Robot Vision, vol. I*. Reading, MA: Addison-Wesley, 1992.
- [29] J. Moody, C. Darken, "Fast learning in networks of locally-tuned processing units," *Neural Computation*, vol. 1, no.2 , pp. 281-294, 1989.

- [30] S. Chen, B. Mulgrew, P. M. Grant, "A clustering technique for digital communications channel equalization using radial basis function networks," *IEEE Trans. on Neural Networks*, vol. 4, no. 4, pp. 570-579, Jul. 1993.
- [31] G. Seber, *Multivariate Observations*. John Wiley, 1986.
- [32] S.R. Peterson, Y.-H. Lee, S.A. Kassam, "Some statistical properties of Alpha-Trimmed Mean and standard type M Filters," *IEEE Trans. on Acoustics, Speech, and Signal Processing*, vol. 36, pp. 707-713, 1988.
- [33] R. V. Hogg, "Adaptive robust procedures: a partial review and some suggestions for future applications and theory," *J. Am. Stat. Assoc.*, no. 348, vol. 69, pp. 909-923, 1974.
- [34] D. M. Titterton, "Estimation of correlation coefficients by ellipsoidal trimming," *Appl. Stat.*, no. 3, vol. 27, pp. 227-234, 1978.
- [35] A. J. Abrantes, J. S. Marques, "A class of constrained clustering algorithms for object boundary extraction," *IEEE Trans. on Image Processing*, vol. 5, no. 11, pp. 1507-1521, 1996.
- [36] I. Pitas, *Digital Image Processing Algorithms*. Prentice Hall, 1992.
- [37] J.-M. Joliot, P. Meer, S. Bataouche, "Robust clustering with applications in computer vision," *IEEE Trans. on Pattern Analysis and Machine Intelligence*, vol. 13, no. 8, pp. 791-802, 1991.
- [38] A. N. Marana, L. da F. Costa, S. A. Velastin, R. A. Lotufo, "Oriented texture classification based on self-organizing neural network and Hough transform," *Proc. Int. Conf. on Acoustics, Speech, and Signal Processing*, pp. 2773-2775, Munchen, Germany, 21-24 April 1997.
- [39] E. Yair, K. Zeger, A. Gersho, "Competitive learning and soft competition for vector quantizer design," *IEEE Trans. on Signal Processing*, vol. 40, no. 2, pp. 294-309, Feb. 1992.
- [40] I. M. Elfadel, R. W. Picard, "Gibbs random fields, cooccurrences, and texture modeling," *IEEE Trans. on Pattern Anal. and Machine Intel.*, vol. 16, no. 1, pp. 24-37, Jan. 1994.

List of Figures

1	Estimation of the ellipse center after trimming.	27
2	Trimming of an ellipse after ordering its data according to the Mahalanobis distance from the center.	27
3	Estimation of a distorted ellipse.	28
4	Description of the algorithm for modeling 3-D objects.	29
5	Estimating the parameters of the Alpha-Trimmed Mean RBF network.	30
6	Modeling a synthetic shape.	31
7	Modeling a noisy synthetic shape.	31
8	Frames from a stack of microscopy images representing cross-sections of tooth pulpal blood vessels and surrounding tissue.	32
9	Vessel segmentation in the selected frames using classical statistics-based RBF training.	33
10	Vessel segmentation in the selected frames using Alpha-Trimmed Mean RBF training.	34
11	3-D representations of microscopy images: (a) original stack of frames; (b), (c), (d) 3-D blood vessel segmentation visualized from three different viewing angles.	35

List of Tables

1	Modeling a synthetic 3-D shape when using LVQ-based RBF, MRBF and Alpha-Trimmed Mean RBF algorithms.	26
---	--	----

Table 1: Modeling a synthetic 3-D shape when using LVQ-based RBF, MRBF and Alpha-Trimmed Mean RBF algorithms.

Algorithm	Noise-free Model		Noisy Model	
	Bias of Center Estimation	Modeling Error (%)	Bias of Center Estimation	Modeling Error (%)
RBF	2.02	11.59	5.38	59.03
MRBF	3.64	27.03	4.30	32.32
Alpha-Trimmed Mean RBF	1.40	5.99	2.93	20.37

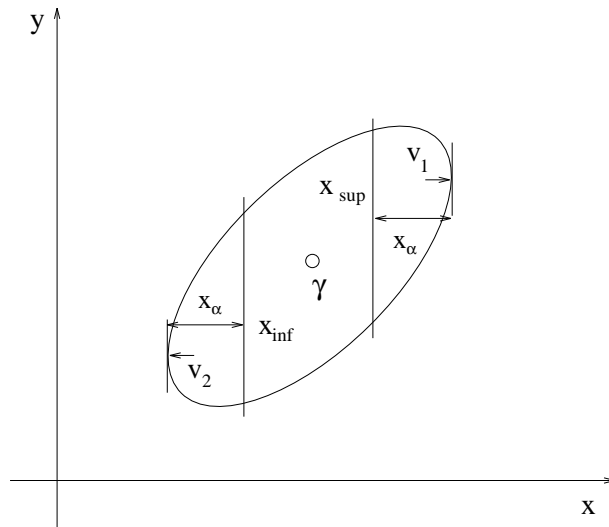


Figure 1: Estimation of the ellipse center after trimming.

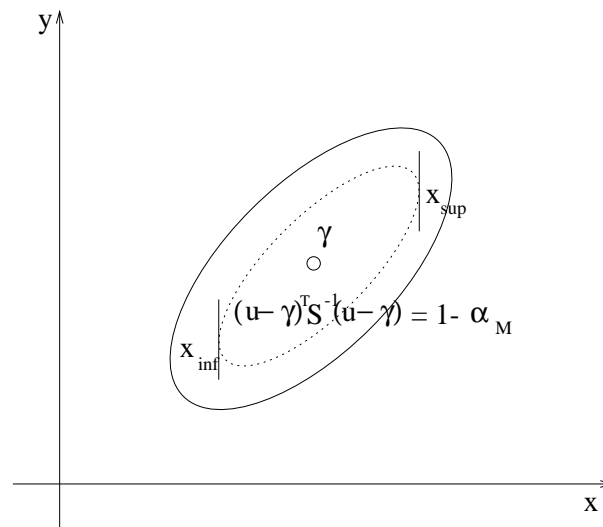
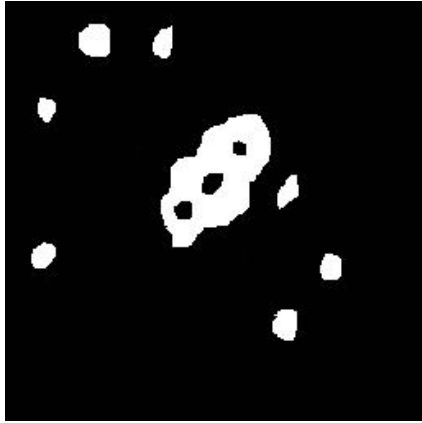
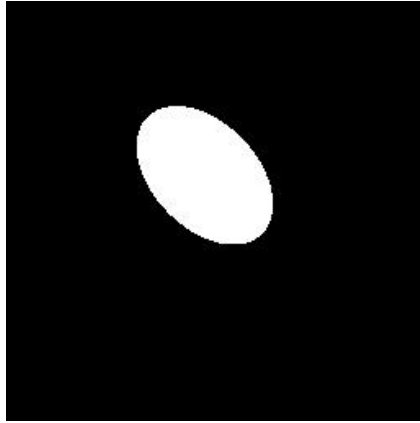


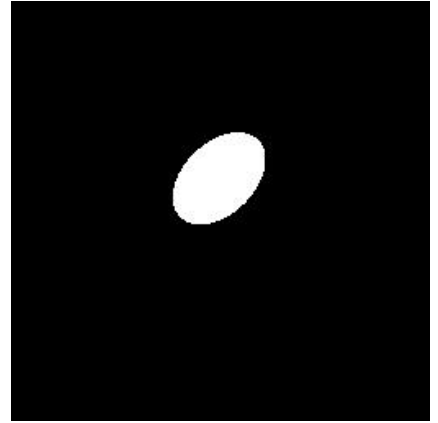
Figure 2: Trimming of an ellipse after ordering its data according to the Mahalanobis distance from the center.



(a) Distorted elliptic shape.



(b) Estimating the ellipse using classical moments method.



(c) Estimating the ellipse using Alpha-Trimmed Mean RBF algorithm.

Figure 3: Estimation of a distorted ellipse.

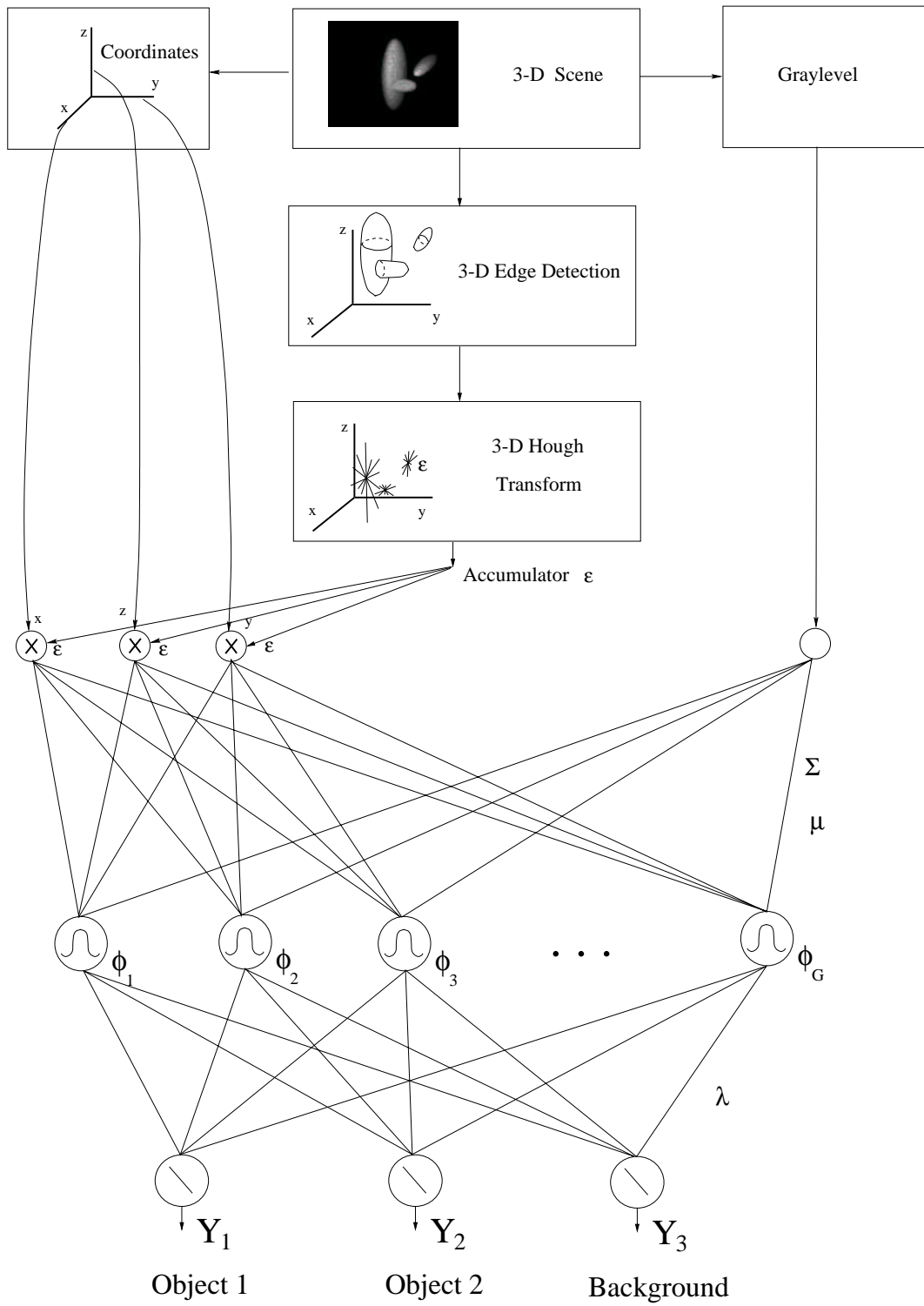


Figure 4: Description of the algorithm for modeling 3-D objects.

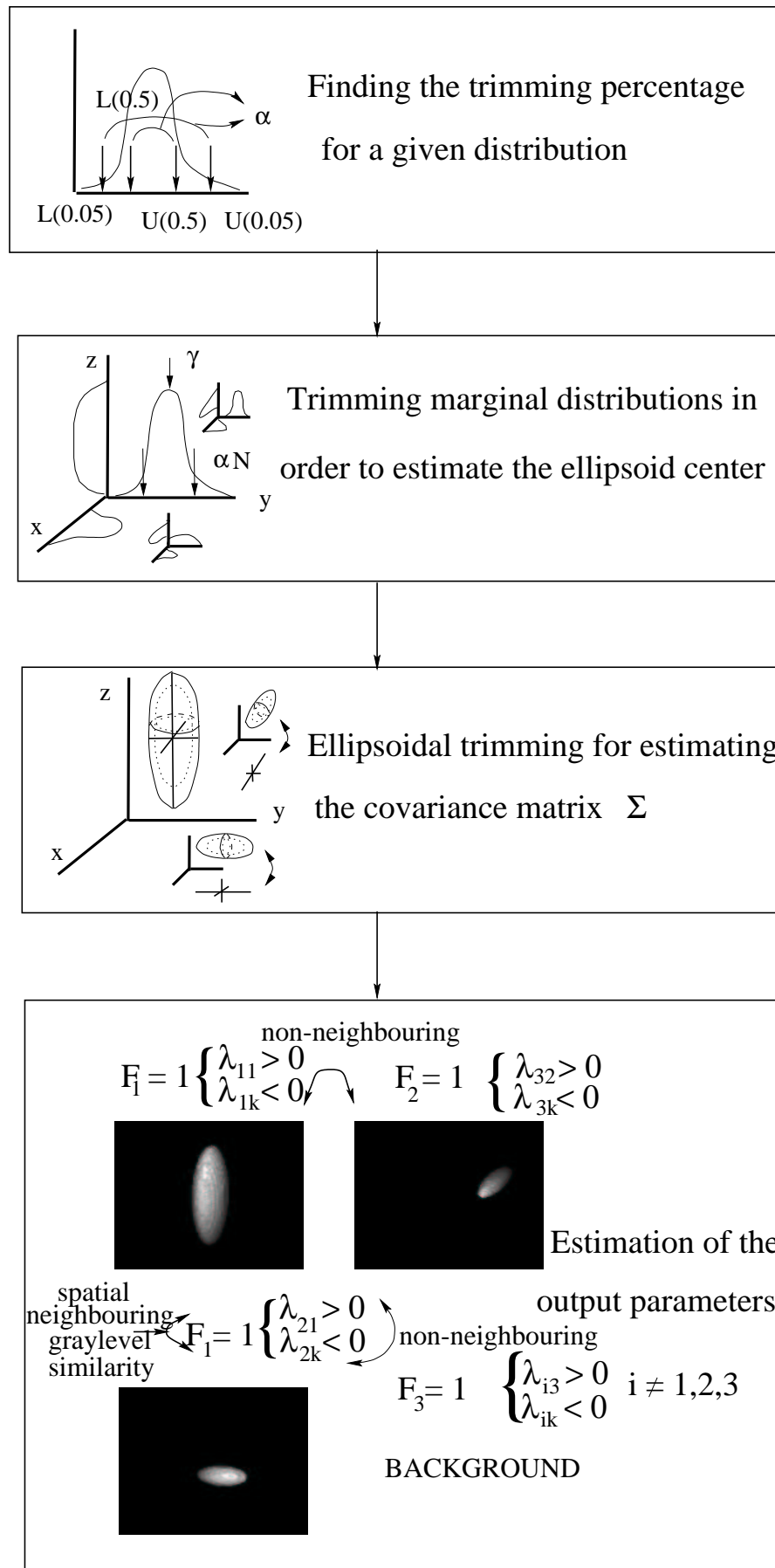
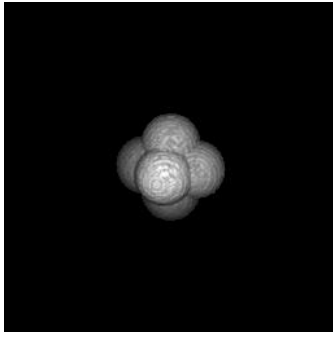
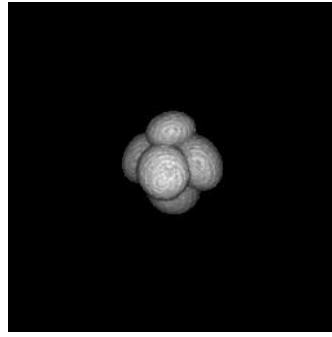


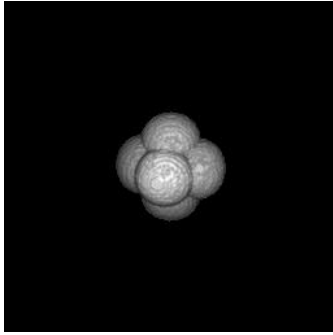
Figure 5: Estimating the parameters of the Alpha-Trimmed Mean RBF network.



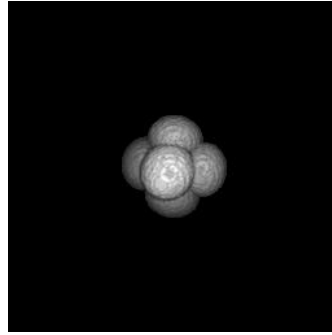
(a) Original shape



(b) RBF modeling

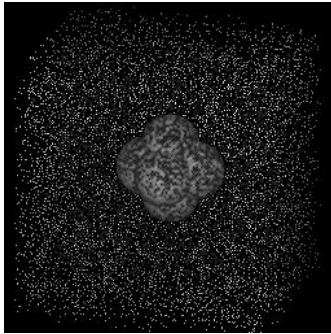


(c) Alpha-Trimmed Mean RBF modeling

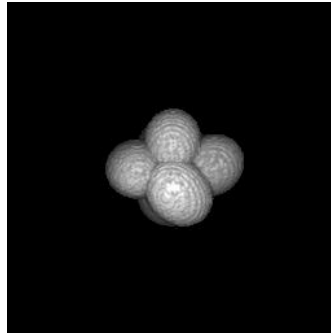


(d) MRBF modeling

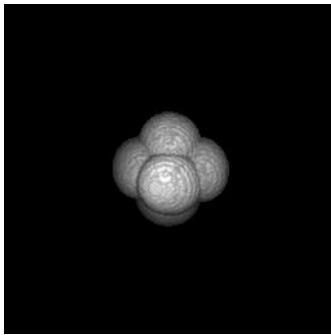
Figure 6: Modeling a synthetic shape.



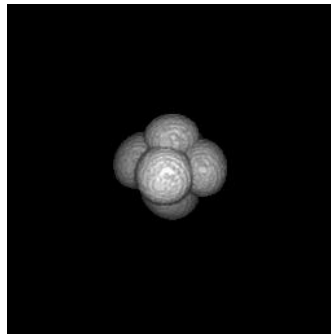
(a) Shape corrupted by noise



(b) RBF modeling



(c) Alpha-Trimmed Mean RBF modeling



(d) MRBF modeling

Figure 7: Modeling a noisy synthetic shape.

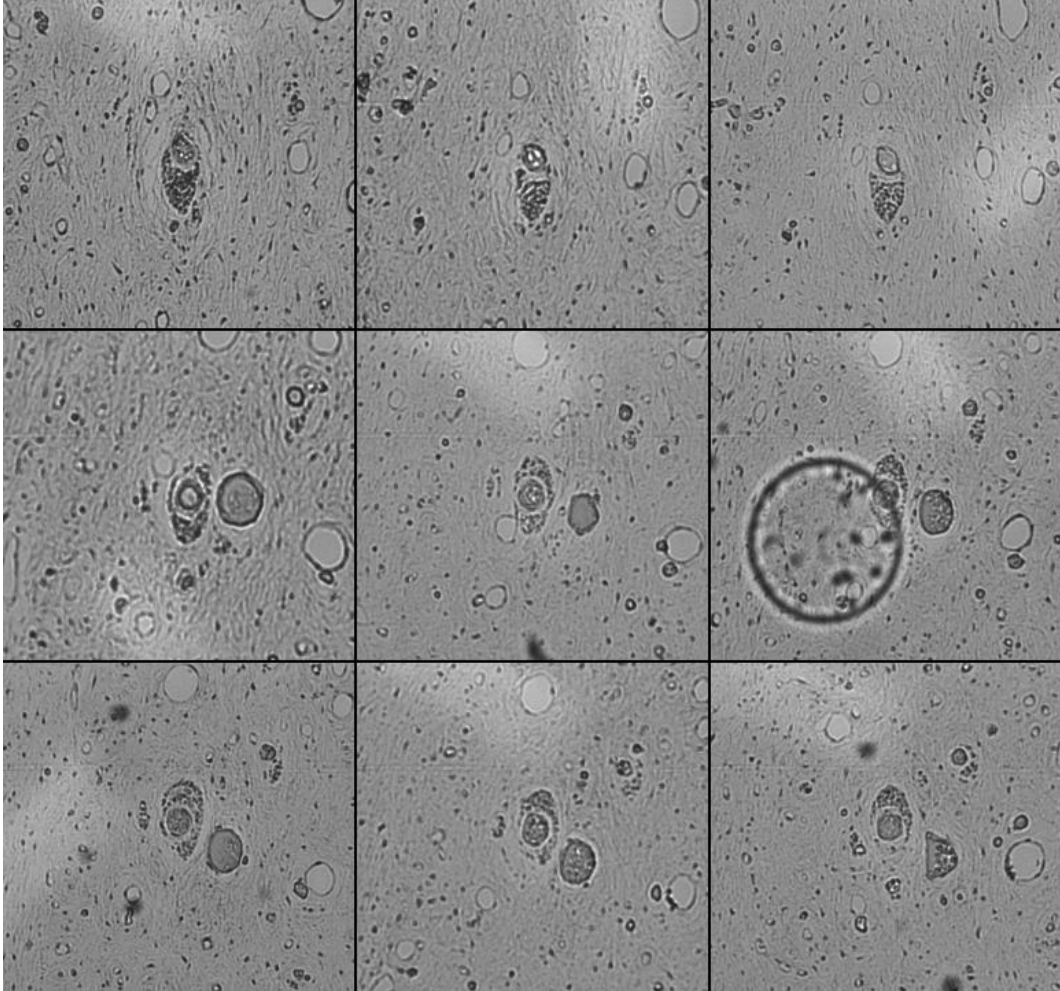


Figure 8: Frames from a stack of microscopy images representing cross-sections of tooth pulpal blood vessels and surrounding tissue.

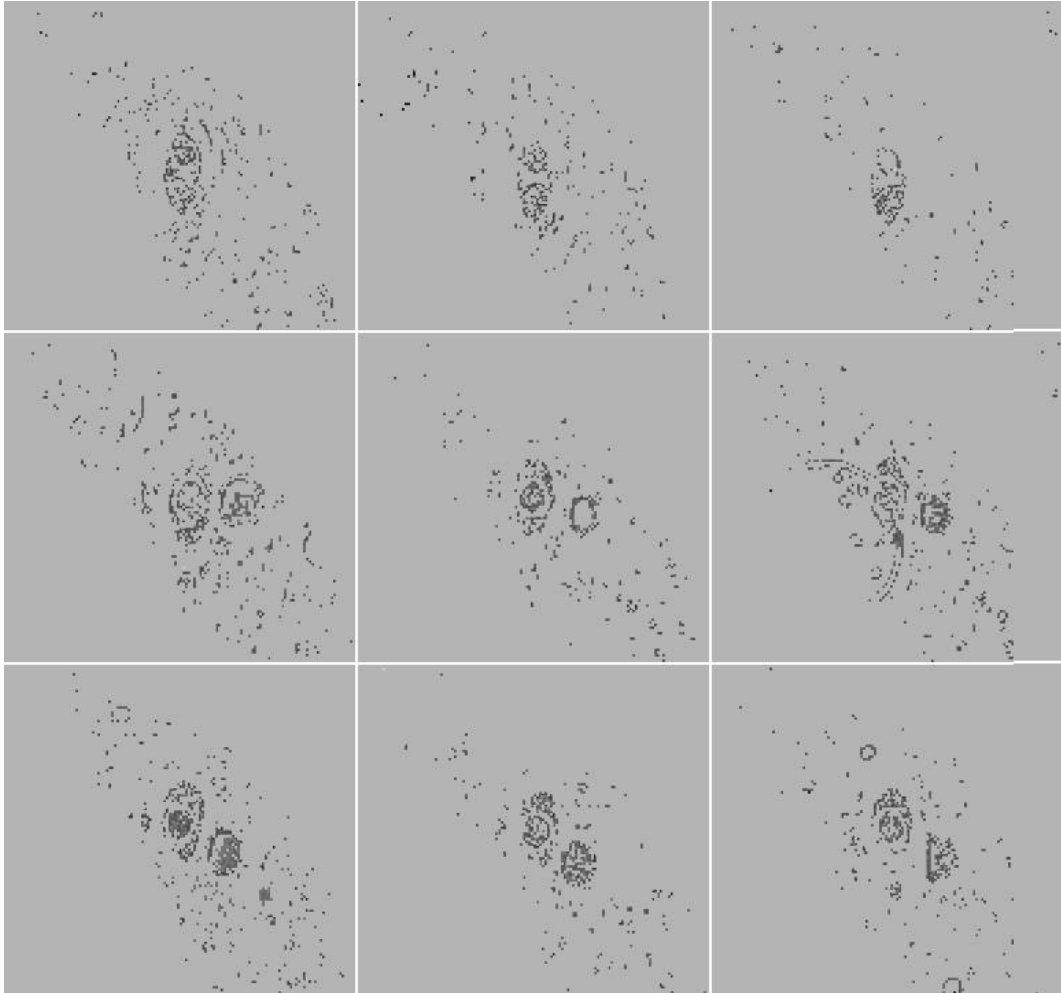


Figure 9: Vessel segmentation in the selected frames using classical statistics-based RBF training.

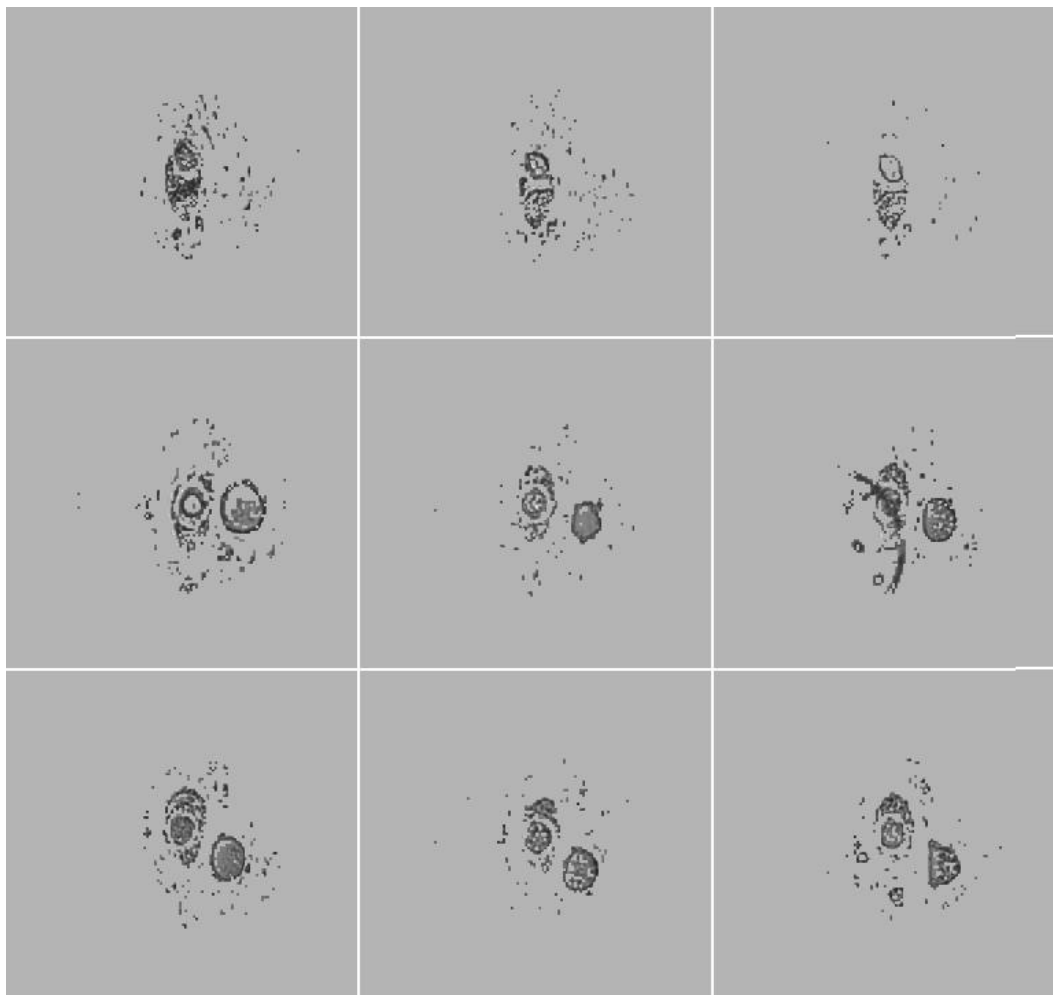
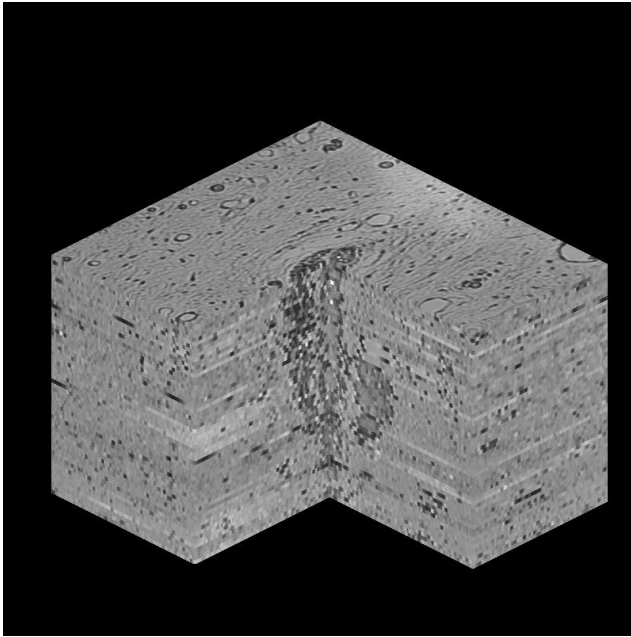
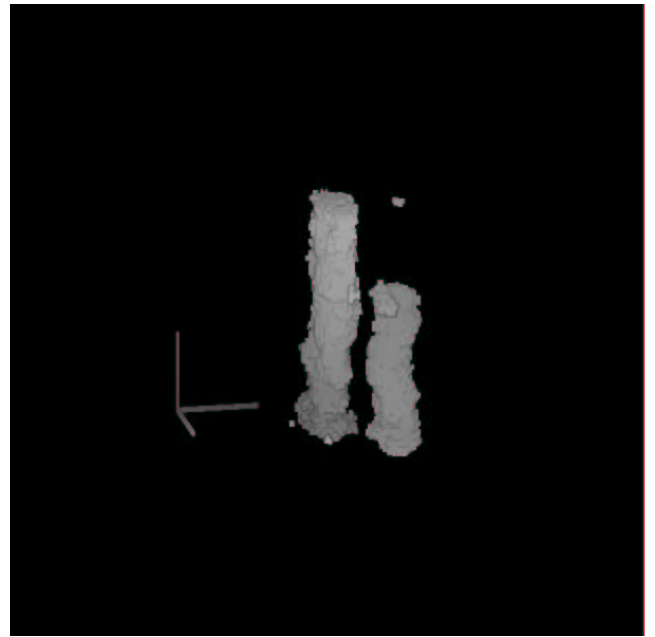


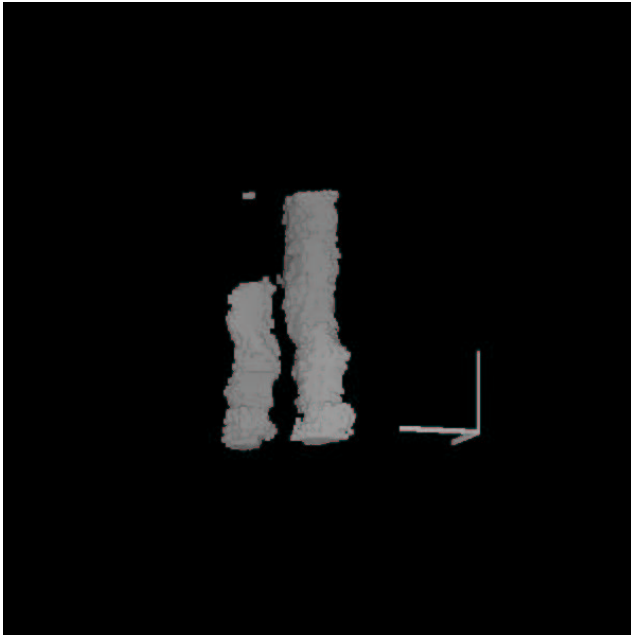
Figure 10: Vessel segmentation in the selected frames using Alpha-Trimmed Mean RBF training.



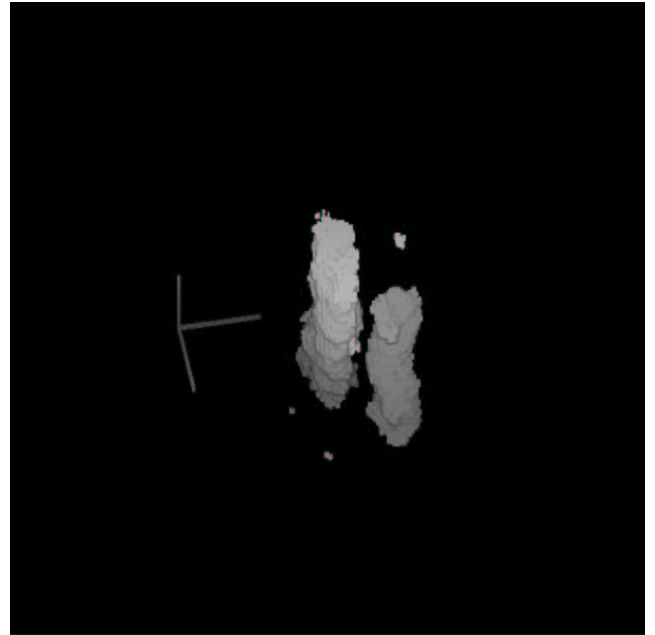
(a)



(b)



(c)



(d)

Figure 11: 3-D representations of microscopy images: (a) original stack of frames; (b), (c), (d) 3-D blood vessel segmentation visualized from three different viewing angles.